When there is a discrepancy between the information in this technical report and information in JDox, assume JDox is correct.

JWST TECHNICAL REPORT

Title:	MIRI Imaging/Coronagraphic Absolute Flux Calibration: 2025 Refinement	Doc #:	JWST-STScI-009289, SM-12#
		Date:	March 11, 2026
		Rev:	
Authors:	Karl D. Gordon	Release Date:	25 March 2026
Phone:	410-338-5031		

1 Abstract

The MIRI imaging and coronagraphic absolute flux calibration has been updated. These updates were motivated by the finding that the year 3 flux calibration monitoring observations required the functional form of the time dependent throughput to be updated to an exponential plus a linear component. All year 3 and the start of year 4 flux calibration observations were added to the previously analyzed commissioning, year 1, and year 2 data. All data was reduced with a development version of the pipeline that included the new photom reference file format now including multiple functional forms for the throughput time dependence. As part of this update, one significant bug and other minor bugs in the analysis scripts were fixed. The significant bug affects all the coronagraphic bands and the FND imaging band, with corrections to these bands ranging from -17.0% to 22.6%, depending on the band. The new photom reference file has been delivered and will be included in the 1.20.0 jwst pipeline and associated crds context release.

2 Introduction

The absolute flux calibration of the MIRI imaging and coronagraphic bands based on commissioning, year 1, and year 2 dedicated observations is presented in Gordon et al. [2025]. Dedicated flux calibration observations are taken every year including repeated observations of the same star every month (years 1–3) or every other month (years 4+) to track throughput variations. The throughput was seen to decrease with time, with the largest decrease seen at the longer wavelengths and with a functional form that was well fit with an exponential. This is similar to, but with a smaller amplitude to the throughput variations seen for the MIRI MRS [Law et al., 2025]. With the year 3 observations, it has become clear that a single exponential does not fully capture

Table 1: New Observations

Name	PID	Subarray	Bands
			ADwarfs
BD+60 1753	6607	SUB256	F560W, F770W, F1000W, F1130W, F1280W, F1500W, F1800W, F2100W, F2550W
	7671	SUB256	F560W, F770W, F1000W, F1130W, F1280W, F1500W, F1800W, F2100W, F2550W
HD 163466	6607	FULL	FND
HD 2811	6604	BRIGHTSKY	F1500W, F1800W, F2100W, F2550W
		FULL	FND
		MASK1550	F1550C
		MASKLYOT	F2300C
			SolarAnalogs
GSPC P330-E	6606	FULL	F560W, F770W, F1000W, F1130W, F1280W, F1500W, F1800W
		MASK1065	F1065C
		MASK1140	F1140C
	7615	FULL	F560W, F770W, F1000W, F1130W, F1280W, F1500W, F1800W
		MASK1065	F1065C
		MASK1140	F1140C

the variations seen[1]. A more complex functional form is needed requiring an different functional form and an updated analysis. This is the motivation for this work. This report gives updates since the Gordon et al. [2025] paper, which gives many details that are not repeated here.

3 Analysis

3.1 New Observations

The new observations include all the year 3 dedicated absolute flux calibration observations and the start of similar observations in year 4. These observations include data of one flux calibration star in each band (PIDs: 6604, 6606, 7615) and of the throughput monitoring star (BD +60 1753) in all the imaging bands (PIDs: 6607, 7671). The specific stars and bands are given in Table 1.

3.2 Data Reduction and Photometry

The data reduction followed that described in Gordon et al. [2025]. A development version of the jwst pipeline that include the new photom reference file format (based on 1.19.1 and represented by PR #9736[2]) and the associated crds context 1416 that notably has updated flat fields. In addition, new mask reference files (dq_init pipeline step) were used (Engesser 2025, JWST Tech. Report, in prep) as they are significantly improved compared to the previous mask reference file.

The measurement of the photometry and calibration factors followed that described in Gordon et al. [2025].

[1] https://www.stsci.edu/contents/news/jwst/2025/updates-to-the-miri-long-wavelength-reduced-count-rate?keyword=MIRI%20count%20rate&itemsPerPage=15&page=1

[2] https://github.com/spacetelescope/jwst/pull/9736

3.3 Time Dependent Functional Form

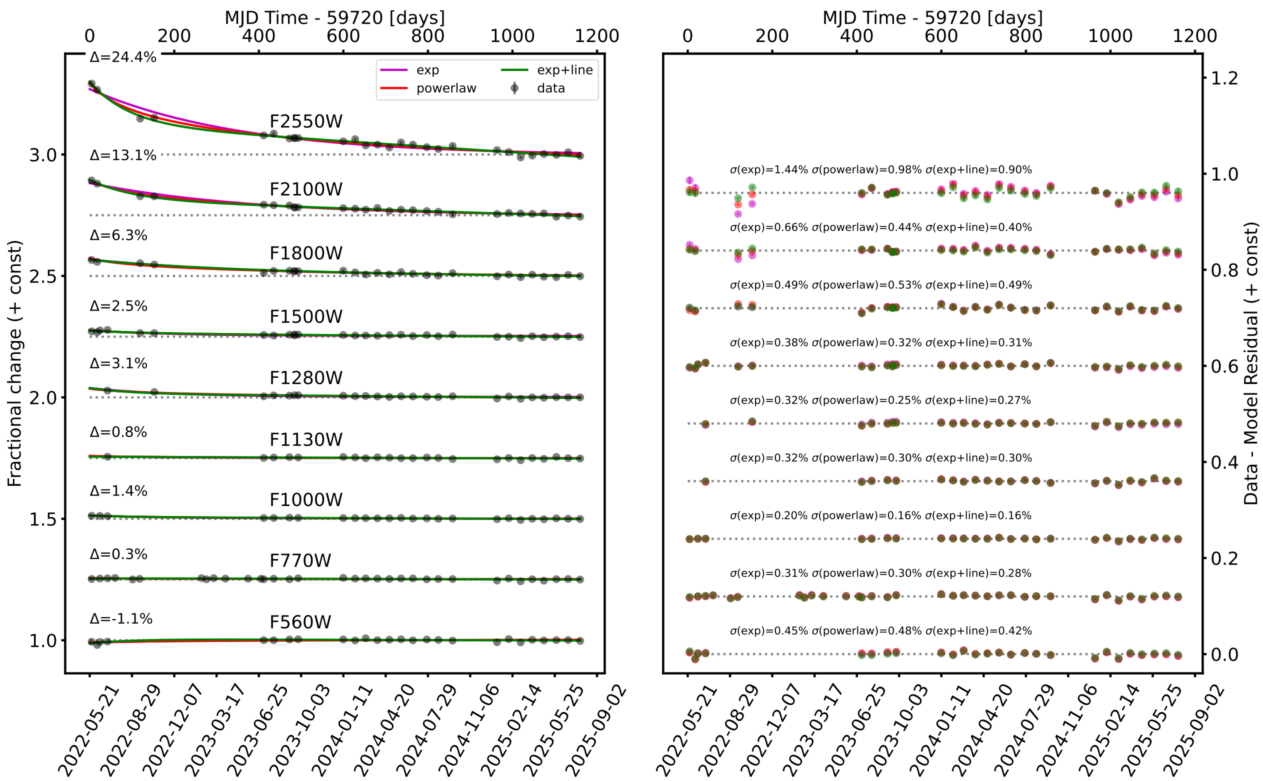

Figure 1: Left: The time-dependent behavior of the repeated observations of BD+60 1753 plus two other stars for all the imaging filters. Three different functional forms fit to the observations in each band are plotted. The dotted line gives the lowest value from the exp+line fit. The change since the beginning of the mission is given as Δ form the exp+line fit. Right: The residuals after subtraction of the exponential model. The σ for each fit and band is given above the residuals.

The temporal dependence of the throughput is shown in Fig. 1 for all the imaging bands. The functional forms fit to the observations are an exponential, powerlaw, and exp+line. For the F2550W data, the original exponential functional form does not provide a suitable fit, over predicting the data at early and late times and under predicting in between. The powerlaw produces a better fit, but still over predicts at early times and over predicts in the middle. The exp+line provides the best fit with the lowest residuals and, hence, this functional form has been adopted for all bands.

There has been one other notable update since Gordon et al. [2025], namely correcting for the different subarrays used for observations at the very beginning during commissioning. Some of the commissioning observations were taken with the FULL subarray, with all the rest of the observations taken with the SUB256 subarray. The difference is small [2%, Gordon et al., 2025], but this is significant and results in a small decrease in the measured Δ and affects the exp+line fit parameters.

3.4 Bug fix

There was a bug found after Gordon et al. [2025] was published that affected the coronagraphic bands and the imaging FND band. In order to “trick” the jwst pipeline into running the CALWEBB_IMAGE3 step – needed for absolute flux calibration – for coronagraphic bands and imaging FND band, the metadata needs to be modified by setting the exposure type (EXP_TYPE) to "MIR_IMAGE" and the filter (FILTER) to the nearest imaging band. This allows the creation of mosaics to remove distortion and fill in missing fluxes from different dithers. An unfortunate side-effect, however, was that the imaging filter, instead of the coronagraphic filter, was used by the photometric flux calibration analysis code to select the aperture, sky annulus, aperture correction, and model fluxes. The F1140C filter has a very similar profile to the F1130W filter, but the incorrect model fluxes used for the F1065C, F1550C, and F2300C bands cause them to have a higher than correct calibration factor, and for the FND band to have a lower than correct calibration factor. This bug was fixed soon after the paper was published as it was seen as a reporting error in the data table for the paper. But the true impact of this bug was not understood until work on the new functional form for the time dependent throughput loss was done.

3.5 Calibration Factors

The updated calibration factor as a function of time and subarray is

$$C(t) = \frac{A}{D_{\rm SA}[1 - B(t - t_o)/365](E_1 \exp[-(t - t_o)/\tau] + E_2)} \quad (1)$$

where t is the time in MJD, A gives the calibration factor at the beginning of the mission, B is the fractional loss per year, E_1 is the amplitude of the exponential term, $t_o = 59720\ d$, τ is the time constant in days, and E_2 is the fractional value of the exponential at infinite time, and $D_{\rm SA}$ is the relative change with subarray. The units of A, B, E_1, and E_2 are in (MJy sr^{-1}) / (DN s^{-1} pixel^{-1}). This updated equation is written such that the time dependence is contained in the denominator and given as a fraction that is one at $t = t_o$ and becomes smaller at later times. Having the time dependence in the denominator aligns with how the jwst pipeline photom step performs the calculation of this factor.

Table 2: Range in $C(t)$ Changes

	Change (%)	
band	min	max
F560W	-0.24	0.81
F770W	0.37	0.83
F1000W	-0.04	0.29
F1130W	-0.38	0.19
F1280W	-0.77	0.02
FND	21.87	22.78
F1500W	0.24	1.00
F1800W	0.17	1.48
F2100W	-0.30	2.58
F2550W	-1.01	2.87
F1065C	-12.50	-12.13
F1140C	-0.12	0.45
F1550C	-7.13	-6.41
F2300C	-17.58	-15.69

The range of percentage changes between the old (2024-08) and new (2025-09) calibration factors for $t_o = 0$ to 1150 days are given in Table 2. These changes include the improved time dependence modeling and additional observations in addition to the bug fix. The main changes are due to the bug fix and are seen in the coronagraphic bands and FND band as expected. The change in the throughput time dependence functional form means that the min and max changes are not necessarily at the beginning or end of the measurements.

Table 3 gives the coefficients for each band where $\sigma(CF)$ is the uncertainty on the calibration factor, $n_{\rm stars}$ is the number of stars included, and σ(repeat) is the uncertainty from the repeatability as

Table 3: Calibration Factor Info

Band	A	B	E_1	τ (days)	E_2	$\sigma(CF)$	$\sigma(CF)$ (%)	$n_{\rm stars}$	σ(repeat) (%)
				Imaging					
F560W	0.4514	0.0023	-0.0189	100.0	1.0189	0.00259	0.57	13.00	0.42
F770W	0.2552	0.0021	-0.0032	100.0	1.0032	0.00064	0.25	13.83	0.28
F1000W	0.3448	0.0025	0.0063	100.0	0.9937	0.00105	0.31	19.00	0.16
F1130W	1.0800	0.0024	0.0002	100.0	0.9998	0.00414	0.38	17.00	0.30
F1280W	0.4063	0.0050	0.0236	100.0	0.9764	0.00138	0.34	16.89	0.27
FND	49.0565	0.0049	0.0231	101.6	0.9769	0.51710	1.05	10.00	
F1500W	0.3604	0.0044	0.0114	140.2	0.9886	0.00170	0.47	21.00	0.31
F1800W	0.4762	0.0049	0.0502	354.7	0.9498	0.00275	0.58	20.00	0.49
F2100W	0.3925	0.0187	0.0745	105.9	0.9255	0.00163	0.42	15.00	0.40
F2550W	0.7158	0.0335	0.1426	93.3	0.8574	0.00684	0.96	16.00	0.90
				Coronagraphy					
F1065C	2.7373	0.0024	0.0034	100.0	0.9966	0.01147	0.42	5.00	
F1140C	2.8537	0.0024	0.0003	100.0	0.9997	0.02123	0.74	5.00	
F1550C	3.5079	0.0045	0.0175	174.0	0.9825	0.01685	0.48	4.00	
F2300C	0.7844	0.0249	0.1031	100.6	0.8969	0.00645	0.82	4.00	

measured from the scatter around the time dependent fit. For the coronagraphic and FND filters, the temporal dependence was calculated by interpolating between the two imaging filters to either side in wavelength and weighting by the distance in wavelength.

Fig. 2 shows the refinement in the calibration factors for each band as a function of time.

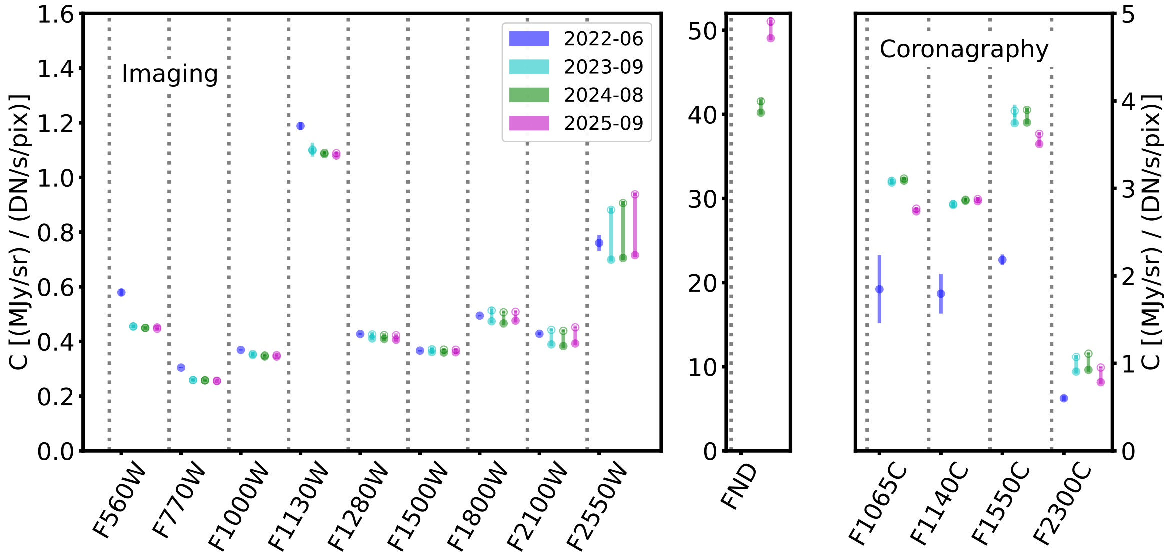

Figure 2: The delivered calibration factors used by the pipeline are plotted versus time. For the three most recent deliveries, the time-dependent variation is shown as a solid symbol (start of observations) connected to an open symbol for $t = t_o + 1200$ days. The changes reflect the improved calibration factor measurements with more observations and a better understanding of the telescope and instrument.

4 Summary

The flux calibration of MIRI imaging and coronagraphy has been updated. These updates are relative to the flux calibration as reported by Gordon et al. [2025]. These updates include:

1. Additional observations including all dedicated flux calibration observations taken in year 3 and observations taken in year 4 through 10 Jul 2025.

2. Reduction of all the flux calibration observations with the development version jwst pipeline that include the new photom reference, crds context 1416, and updated bad pixel masks.

3. Updating the time dependence throughput functional form from an single exponential to a linear and exponential. This included applying the appropriate subarray correction for the observations of the monitoring star in commissioning.

4. Fixing a bug in the analysis code that incorrectly reported the filter for the coronagraphic (F1065C, F1140C, F1550C, & F2300C) and FND imaging bands. This bug resulted in incorrect calibration factors in previous version of the photom reference file.

5. Updated flux calibration including the exp+linear throughput functional form functional is available in the jwst pipeline since version 1.20.0.

References

Karl D. Gordon, G. C. Sloan, Macarena Garcia Marin, Mattia Libralato, George Rieke, Jonathan A. Aguilar, Ralph Bohlin, Misty Cracraft, Marjorie Decleir, Andras Gaspar, and et al. The James Webb Space Telescope Absolute Flux Calibration. II. Mid-infrared Instrument Imaging and Coronagraphy. *AJ*, 169(1):6, January 2025. doi: 10.3847/1538-3881/ad8cd4.

David R. Law, Ioannis Argyriou, Karl D. Gordon, G. C. Sloan, Danny Gasman, Alistair Glasse, Kirsten Larson, Leigh N. Fletcher, Alvaro Labiano, and Alberto Noriega-Crespo. The James Webb Space Telescope Absolute Flux Calibration. III. Mid-infrared Instrument Medium Resolution Integral Field Unit Spectrometer. *AJ*, 169(2):67, February 2025. doi: 10.3847/1538-3881/ad9685.

A Appendix

The calibration factors for all the bands as a function of time are show in Fig. 3 after correction for the subarray and time dependencies.

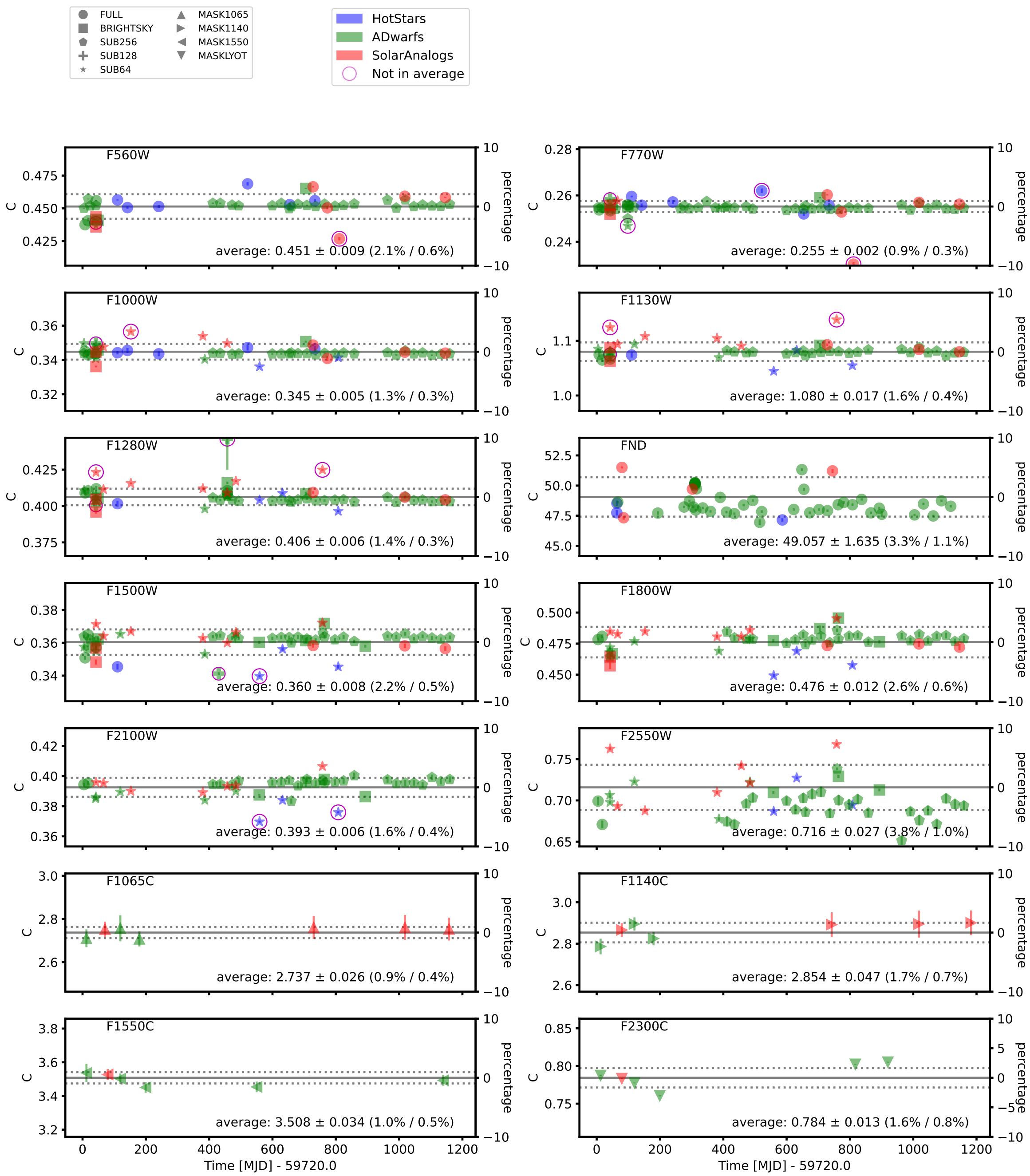

Figure 3: The calibration factors as a function of observation time for every observation for the imaging and coronagraphic filters. The temporal response loss and subarray variations have been corrected. While the observations of HD 180609 are within the scatter for some bands, it is flagged in all bands and not used. In addition, some observations are flagged as $> 3.5\sigma$ from the weighted average and not used. A horizontal solid gray line and the parallel dotted lines give the weighted average $\pm 1\sigma$ standard deviation. The calibration factors and uncertainties are given in the lower right of each plot, and the percentage standard deviation and standard deviation of the mean are given in parentheses as well. Each star (not observation) has equal weight in the average calibration factor calculation.